Recent fluctuations in the extent of the firn area of Austfonna, Svalbard, inferred from GPR

Thorben DUNSE,[1] Thomas Vikhamar SCHULER,[1,2] Jon Ove HAGEN,[1] Trond EIKEN,[1] Ola BRANDT,[3] Kjell Arild HØGDA[4]

[1] *Department of Geosciences, University of Oslo, P.O. Box 1047, Blindern, NO-0316 Oslo, Norway*
E-mail: thorben.dunse@geo.uio.no
[2] *Norwegian Water Resources and Energy Directorate, P.O. Box 5091 Majorstua, N-0301 Oslo, Norway*
[3] *Norwegian Polar Institute, Polar Environmental Center, N-9296 Tromsø, Norway*
[4] *Norut IT, P.O. Box 6434, Forskningsparken, N-9294 Tromsø, Norway*

ABSTRACT. In spring 2004 to 2007 we conducted ground-penetrating radar (GPR) measurements on the Austfonna ice cap, Svalbard, with the original aim to map the thickness and distribution of winter snow. Here, we further exploit the information content of the data and derive a multi-year sequence of glacier-facies distribution that gives valuable spatial information about the total surface mass balance (SMB) of the ice cap, beyond the usually evaluated winter balance. We find that following an initial decrease in the extent of the firn area (2003 to 2004), the firn line lowered within two subsequent years by about 40 to 100 m elevation in the north and west, and 150 to 230 m in the south and east of the ice cap, corresponding to a lateral expansion of the firn area along the profiles by up to 7.3 and 13.3 km, respectively. The growth of the firn area is in line with stake measurements from Etonbreen that indicate a trend towards less negative SMB over the corresponding period.

INTRODUCTION

Mass losses from glaciers and ice caps outside Antarctica and Greenland are estimated to have accounted for 0.50 ± 0.18 mm a^{-1} of the observed rate of global sea-level rise from 1961 to 2003 and 0.77 ± 0.22 mm a^{-1} for 1993-2003 (IPCC, 2007). The large uncertainty associated with these estimates calls for more accurate and spatially distributed measurements of glacier mass balance. In order to cover the entire polar regions, surface mass balance (SMB) observations are carried out from space (Shepherd and Wingham, 2007; Zwally and others, 2005). One standard method to determine mass changes is provided by satellite radar altimetry. Surface elevation measurements are taken over several time intervals to yield volume changes (Wingham and others, 2001). However, this technique is sensitive to ice topography and radar returns from beneath the surface (Scott and others, 2006) and relies on ground-truth data. Volume backscatter that originates from inhomogeneities within the snow and firn leads to ambiguities in the detection of the surface reflection. Furthermore, knowledge of variations in snow and firn density is critical for accurate conversion of volume changes to mass changes. Both factors need particular consideration in areas where meltwater retention by refreezing is significant and highly variable in space and time.

The SMB of a glacier is reflected in the spatial distribution of its glacier facies. Following the usual textbook definition by Paterson (1994), areas exclusive of snow melt are referred to as dry snow facies, generally restricted to the interior of Greenland and Antarctica. The upper accumulation area of Arctic ice caps typically consists of the percolation facies. Here, surface melt occurs during the summer period and meltwater produced at the surface (or rain) infiltrates into the snow, where it refreezes. If, by end-of-summer, the entire snowpack reaches pressure melting point, the area is referred to as wet snow facies. Here, meltwater might percolate below the last summer surface (LSS) into older layers of firn. The combined area of wet snow, percolation and, where applicable, dry snow facies, is often referred to as firn area. At the lower end of the firn area follows the superimposed ice (SI) facies. That is ice, formed at the base of the snowpack on top of impermeable cold ice, whereas ice layers, lenses and glands within the snow and firn are termed internal accumulation (Hagen and Reeh, 2004). For many Arctic glaciers, accumulation by internal refreezing and SI formation may be spatially and temporally highly variable, but generally represents a significant contribution to the SMB (Hagen and others, 2003; Woodward and others, 1997). This variability is expressed by changes of the glacier facies distribution, and emphasizes the importance of ground truth data for analysis of space-borne data, especially if collected over Arctic glaciers and ice caps. As glacier facies arise from metamorphism and ablation of the winter snow, they relate to both winter and summer conditions.

Field studies of SMB often involve ground-penetrating radar (GPR) surveys at antennae frequencies around 400-1500 MHz (P and L-band) with the primary goal to map the distribution of snow (Taurisano and others, 2007; Kohler and others, 1997). The density contrast at the LSS causes an internal reflection horizon (IRH) that can be tracked along continuous profiles. Given adequate post-processing of the data, GPR also enables detailed studies of the near-surface firn stratigraphy (e.g., Dunse and others, 2008), as well as it provides a non-destructive method to map glacier facies (Brandt and others, 2008; Wadham and others, 2006). This technique has been used for validation of glacier facies inferred from synthetic-aperture radar (SAR) data (Langley, 2007; Langley and others, 2007), but so far not been directly applied as a tool of glacier monitoring.

In this study we present GPR data collected at 800 MHz along some 250 km of profiles across the Austfonna ice cap. We re-analyze GPR data from spring 2004 and 2005, published by Taurisano and others (2007) and extend their time series by including measurements from spring 2006 and 2007. For each year, the thickness of the winter snow is mapped and the glacier facies beneath the winter snow are identified. In doing so, we produce a multi-year sequence of glacier-facies distribution.

STUDY SITE

Austfonna is a polythermal ice cap, situated on Nordaustlandet, Svalbard. Centered at 79.7°N and 24.0°E it covers an area of 8120 km^2 (Figure 1). The ice cap has a simple dome-shaped topography with well defined drainage basins, several of which exhibit surge-type behavior (Dowdeswell and others, 1999; Hagen and others, 1993). The maximum elevation of about 800 m a.s.l. in the central part coincides with the maximum ice thickness of about 580 m (Dowdeswell, 1986). 28 % of Austfonna's bed lies below sea level and along a large portion of its boundary, it is calving into the Barents Sea.

A number of investigations have been made during previous years with focus on elevation changes and mass balance. Pinglot and others (2001) inferred the annual mean SMB of the accumulation area of Austfonna for the period 1986 to 1998/1999 from shallow ice cores dated by the detected radioactive fallout horizon from the Chernobyl accident. Maximum values of around 0.5 m w.e. a^{-1} were measured in the summit area. Taurisano and others (2007) mapped the winter snow cover using GPR data collected in spring 1999, 2004 and 2005. As Pinglot and others (2001), they found an asymmetry in SMB, in accordance to the distribution of snow, with twice as much accumulation in the southeast than in the northwest. Both studies conclude that this pattern results from the proximity of the Barents Sea in the east, southeast, providing a significant moisture source for precipitation. Taurisano and others (2007) related snow thickness to all three spatial coordinates by multiple regression to derive an accumulation index for further use in a SMB model by Schuler and others (2007). The distribution of snow across Austfonna is thus relatively well understood, whereas the fate of the snow throughout the summer-melt season is only known at a few points from shallow cores and mass balance stakes. Therefore, large uncertainties remain with the spatial and temporal variability of the firn-area extent, as well as the formation of SI and, hence, estimates of the equilibrium-line altitude (ELA).

Using airborne laser altimetry conducted in 1996 and 2002, Bamber and others (2004) showed that Austfonna is thinning at lower elevations and thickening in the interior, and explain this by an increase in accumulation. Hagen and others (2005) point out that elevation changes may be driven by both surface processes (accumulation and ablation) or ice dynamics (possible build-up towards surge activity). Bevan and others (2007) suggest that slow ice dynamics is the key factor for the positive mass balance of the accumulation area, since the actual volume flux across the equilibrium line is only half of the balance flux.

DATA ACQUISITION AND PROCESSING

Annual field studies were conducted in spring 2004 to 2007 with data collection over two-week periods in late April, early May. GPR and GPS data was collected along four major transects that cross the ice cap in different orientations with a total length of about 250 km (Figure 1). The start and end positions along the transects differ in-between years by up to 5 km, while the lateral offset is generally smaller than 10 m. Due to logistical and technical problems, no GPR data was collected south and south-eastwards from the summit in 2005 and some data gaps occurred in 2006. GPR and GPS surveys were complemented by snow pit investigations (usually 2 to 4 pits for each transect in a particular year) and manual snow-depth sounding (every ∼2 km) using ordinary avalanche probes. Snow pits were excavated down to the LSS. In the ablation and SI area, the LSS was recognized as the snow-ice interface, wile in the firn area the LSS appears as either a distinct ice layer or a transition towards large refrozen ice crystals (>3 mm). At some locations in the firn area, the snow pits were extended by 0.5 m below the LSS. The bulk density was measured at 20 cm intervals, and snow stratigraphy, temperature, crystal size and hardness were logged.

Ground-penetrating radar and GPS

The GPR data was collected using a commercial impulse-radar system (RAMAC, Malå GeoScience) with shielded antennae at a frequency of 800 MHz. A GPS (GNSS) receiver was operated together with the GPR for simultaneous kinematic positioning. The GPR control unit and the GPS system were mounted on one sledge, the GPR antennae on a separate unit made of fibre glass, and pulled by a snowmobile. A driving speed of around 5 m s^{-1} and a constant triggering rate of the GPR resulted in a trace interval of 0.25 to 0.30 m. The receiving timewindow was set to 145 ns in 2007 and 126 ns in previous years, in order to image a depth range of at least 10 m. Every trace consists of 1024 samples corresponding to a sample interval of 0.14 ns and 0.12 ns respectively. GPS measurements were logged at a rate of 1 Hz, and post-processed using a stationary GPS as reference. The accuracy of the post-processed GPS data is estimated to be typically better than 10 cm in all three spatial coordinates. Positions of individual traces were allocated by linear interpolation between the post-processed GPS coordinates.

Post-processing of the GPR data included static correction and frequency filtering. Constant time-delay clutter and system artifacts were eliminated using a horizontal filter. For visualization and interpretation of the data a gain function (energy-decay type) was applied.

During data acquisition in spring the snow was entirely at sub-freezing temperatures. Effects of liquid water on the propagation of the radar signal are therefore neglected. The wave speed v of the radar signal in dry snow was derived from the permittivity ε'_r,

$$v = \frac{c}{\sqrt{\varepsilon'_r}} ,$$

with c the speed of light in vacuum. We used the empirical relation of Kovacs and others (1995), to relate snow density (kg m^{-3}) to permittivity:

$$\varepsilon'_r = (1 + 0.000845\rho)^2 .$$

We derive the snow thickness using the two-way traveltime (TWT) of the reflection occurring at the LSS and the wave

speed. In-situ information of snow depth from manual soundings and snow pits ensure that the correct IRH is associated with the LSS.

The error in the depth determination of the LSS mainly arises from lateral variability of the bulk-snow density, and hence wave speed, from the applied constant velocity. In 2007, bulk densities from measurements at 14 snow pits yielded a mean value and related standard deviation of 390 ± 21 kg m^{-3}. Applying the above equations yields a wave speed of 2.25 ± 0.03 m μs^{-1}. Values for the other years were determined following the same procedure.

The GPR system is designed such that the center frequency corresponds approximately to the bandwidth. The wavelength λ in firn ($\rho = 600$ kg m^{-3}) is $\sim$0.25 m. The theoretical resolution of $\lambda/4$ is therefore about 0.06 m. However, this is limited by the length of the transmitted wavelets, comprising 2 cycles (approximately 2.5 ns), as interference of partial reflections from inhomogeneities within the length of the wavelets occur. The effective interface resolution hence equals the wavelength, which for our domain varies from 0.21 m for glacier ice ($\rho = 900$ kg m^{-3}) to 0.29 m for windpacked snow ($\rho = 370$ kg m^{-3}).

Additional data sets

In 2007, vertical density profiles were obtained using a neutron-scattering probe (Morris and Cooper, 2003). Measurements were made while retrieving the probe from the bottom of a borehole. A radioactive source in the probe emits fast neutrons, which are slowed down by scattering as they move through the snow, firn or ice. Density profiles were determined from the measured count rate of slow neutrons returning to a detector within the probe (Morris, 2008). The count rate depends on the characteristics of the probe, the snow/firn/ice density, temperature and the diameter of the borehole (Hawley and others, 2008). The probe has a theoretical resolution of 1 cm. However, due to the relatively low number of returning neutrons it was necessary to increase the counter length to 13 cm. This means the recorded density profile represents a running average over 13 cm and thin ice layers or other abrupt density changes will not be correctly resolved. The boreholes were located within 100 m^2 in the vicinity of the basecamp (79.94°N, 24.24°E) at an elevation of 775 m a.s.l. and at Cry1 (79.85°N, 23.80°E) at an elevation of 659 m a.s.l. (Figure 1). The boreholes reached depths of 8 to 14 m. The vertical density profiles obtained from the boreholes cover all or a major portion of the GPR depth range and serve as validation of the conclusions drawn from the GPR data.

In order to compare the field measurements with an independent data set, we employed data from the Advanced Synthetic Aperture Radar (ASAR) instrument onboard the European Space Agency satellite, Envisat. ASAR operates in both ascending and descending orbits and with different look angles and polarization combinations at a center frequency of 5.3 GHz (C-band). We selected all scenes (approximately 80) that covered the entire of Austfonna during winter 2005 to 2007 (October to April). During the winter season the snow is dry and has therefore little impact on the on the C-band backscatter (Langley and others, 2007). The individual scenes were calibrated and geocoded using an algorithm by Norut Tromsø, Norway, (Lauknes and Malnes, 2004) resulting in multilook images with 100 m resolution in both range and azimuth. The individual scenes were then averaged to produce a single 2D backscatter image.

In 2004 a network of mass balance stakes distributed over the ice cap was established. Several stakes were successfully re-measured in the following years, enabling calculation of specific SMB figures at these locations. The winter balance is given directly by the snow water equivalent of the winter snow, while the total SMB is assessed from changes in stake height above the LSS and the snow water equivalent.

MAPPING OF GLACIER FACIES

Glacier facies relate to the surface properties of a glacier and are an expression of its SMB. Brandt and others (2008), Langley (2007) and Wadham and others (2006) showed the potential of the GPR to map various glacier facies.

The accumulation area is characterized by either firn or SI. On Austfonna, the firn facies consists of wet snow. In certain years, some snow in the summit area might remain at sub-freezing temperatures throughout the entire summer, and a percolation facies may form. The ablation area is typically composed of pure glacier ice. Firn, SI and glacier ice are recognized by their characteristic signal-reflection pattern (Figure 2) dependent on typical occurrence and strength of dielectric contrasts (Brandt and others, 2008). Due to its homogeneous properties, pure, cold glacier ice is predominantly transparent to electro-magnetic waves and signal reflections barely occur. In the firn area, the strong dielectric contrast between solid-ice clusters and an often coarse-grained firn matrix cause IRHs of strong amplitudes, while a varying air-bubble content in the SI causes IRHs of lower amplitude.

We use these properties to map the facies underneath the winter snowpack: firn (F), SI and glacier ice of the ablation area (GI) (Figure 2). We further sub-categorize the classification F into a long-term firn area (F1); a firn layer that originates from multiple years of accumulation, but lies in a zone of recent ($\sim$10 years) variability of the firn line (F2); and a thin firn layer that apparently originates from one accumulation season only (F3). Regions where strong IRHs indicate firn over most of the depth range of the GPR image (6 m and more, corresponding to $\sim$10 or more mass balance years) are classified as the long-term firn area. IRHs in F2 typically show a larger spatial variability than in F1 and typically converge with the LSS at lower elevations. IRHs in the SI area generally show an even larger spatial variability. The formation of SI requires ponding of free water and is therefore strongly controlled by local topography (Brandt and others, 2008). According to the above definition, direct transition from F2 to SI is possible. Transition from SI to F2, on the other hand, involves at least two consecutive years of firn accumulation at a particular location. SI has to be initially covered with a thin layer of firn in one year (F3), to reach the F2 classification in the subsequent year.

In the following, the term glacier facies always relates to the glacier facies beneath the winter snowpack. GPR measurements in spring (year n) therefore yield the thickness of the winter snow accumulation (year n) and the extent of the glacier facies at the end of the previous summer (year $n-1$). Measurements of snow accumulation are related to the winter balance, only. Glacier facies result from a combination of snow accumulation and subsequent metamorphism and ablation of the winter snow cover. Therefore, the above method of detecting glacier facies also provides a measure of summer conditions. In re-analyzing the GPR data from 2004 to 2007, we derive a multi-year sequence of glacier-facies distri-

bution along the transects that allows us to study their inter-annual fluctuations. It should be noted, that the classification of GPR data is a somewhat subjective process. However, the same processing has been applied to the entire data set and the classification was performed by a single person to ensure consistent interpretation.

VALIDATION

To gain more confidence in our interpretation of the GPR data, we first compare the GPR images with the vertical density profiles from neutron probing, and find a clear relation between the observed density profiles and the signal-reflection pattern in the radar image. We then compare the GPR-derived glacier facies with radar zones in the SAR image of Austfonna.

Neutron-scattering probe

The six density profiles recovered at the basecamp are shown in Figure 3a. The site falls in an area classified as F1, the long-term firn area. The winter snowpack is characterized by densities between 350 and 450 $\mathrm{kg\,m^{-3}}$, in agreement with measurements in a nearby snow pit. The LSS is recognizable as a sharp density increase at approximately 14 ns TWT, corresponding to a depth of 1.7 m. The digitized LSS from GPR is at the same depth (Figure 3b). From the LSS down to 33 ns the densities are in the range 470 to 570 $\mathrm{kg\,m^{-3}}$, which are typical for firn. Values in the range of 550 to 850 $\mathrm{kg\,m^{-3}}$occur between 33 and 60 ns and indicate firn and ice layers. In the GPR image, this depth range is characterized by strong reflection amplitudes, without resolving individual IRHs. At around 60 ns (∼6 m depth) the firn-ice transition is reached. Below this depth range, the density varies around 860 $\mathrm{kg\,m^{-3}}$, and the signal reflections in the GPR image are much weaker.

The classification at Cry-1, north of the summit, is F3 for summer 2005 and F2 for 2006. The neutron-probe profile reveals densities between 500 and 630 $\mathrm{kg\,m^{-3}}$ from the LSS at 13 ns down to 22 ns TWT (Figure 3c). Below, the density sharply increases to approximately 850 $\mathrm{kg\,m^{-3}}$ indicating the firn-ice transition at a depth of about 2.4 m. In the GPR data, the transition produces an IRH at that depth (Figure 3d), separating a region with strong reflection amplitudes above (firn) from low ones below (ice).

SAR-radar zones

To compare the backscatter zones of the SAR image with the GPR results, we plot the colour-coded glacier facies, inferred from GPR, on top of the 2D backscatter image (Figure 4). The backscatter intensities of the SAR signal represent an integral of all backscatter sources from the illuminated volume (König and others, 2002). While the dry winter snow has only only minor effects on the SAR signal, the properties of the firn and ice below the LSS control the penetration depth of the signal. In the firn area, volume scatter from inclusions of solid ice clusters dominates and results in high backscatter intensities (light gray shades/white). In the ablation area, volume backscatter from relatively homogeneous glacier ice is insignificant and a distinct snow-ice interface leads to specular reflection of energy away from the side-looking instrument, resulting in low backscatter intensities (dark gray shades). SI is characterized by a varying air-bubble content that causes medium backscatter intensities.

Most striking feature of the comparison is that sections of the GPR transects classified as F1 fall within the limits of the high-backscatter area. Furthermore, the transition between F1 and F2 coincides with the boundary that separates areas of high backscatter from areas of medium backscatter. Sections of the GPR transects classified as GI coincide with areas of low backscatter. The good agreement with the SAR data gives further confidence in the GPR-based glacier-facies classification, as previous studies of glacier-facies classification showed that both SAR and GPR systems yield very similar results (Brandt and others, 2008; Langley, 2007).

RESULTS

The observed distribution of snow accumulation in 2006 and 2007 reconfirms the asymetric snow distribution found by Taurisano and others (2007) and Pinglot and others (2001). Figure 5 shows two transects running from the western to the eastern margin. In the four-year period 2004 to 2007, the snow thickness typically varies from 0.5 to 1.5 m in the west, and 1.5 to 3 m in the east. The lowest snow accumulation was measured in spring 2004, with a mean thickness of 1.21 m over the entire length of the two transects. In spring 2006, a mean thickness of 2.01 m was measured over the same distance.

Glacier facies and their temporal variation

Collected in spring 2004 to 2007, the GPR data yields the extent of the glacier facies in end-of-summer 2003 to 2006. We investigate fluctuations during this period by plotting the colour-coded facies on top of a contour map of Austfonna (Figure 6). The most striking feature is a significant increase in the extent of the firn area, starting winter 2004/2005. In 2003 and 2004, the firn facies was confined to the summit area and SI was exposed along large portions of the transects (Figure 6a,b). In the subsequent two years, SI became to a large extent covered by firn (Figure 6c,d). We further note firn pockets (F2) within the upper parts of the SI in 2003, which were not longer present in 2004. The lower boundary and the total change of the firn area, both in vertical and lateral dimension are listed for each profile in Table 1. No differentiation has been made, whether or not the firn originates from the previous year. In addition, estimates of the equilibrium-line altitude inferred from the mass balance stakes on Etonbreen are provided. Between 2003 and 2006, the firn line decreased by about 40 to 100 m elevation in the north and west of Austfonna, 150 to 230 m in the south and east, respectively. This corresponds to a lateral expansion of the firn area by up to 7.3 km along profiles in the north and west and up to 13.3 km for the southern and eastern profiles.

To visualize the inter-annual changes in more detail, and to allow direct comparison between measurements from different years we select a transect along which data was collected in all years. We plot the extent of the glacier facies along the profile that runs from Etonbreen in the west via the summit towards the east (Figure 7). The increase of the area classified as F2 or F3 in the period summer 2004 to summer 2006 is clearly seen. For each year, a progressively larger portion of the sections classified as SI is covered by an expanding and thickening layer of firn. However, the sections with deep firn F1 show little inter-annual variation. This highlights the fact that F1 originates as an integral of many years of firn accumulation. The only notable change in the extent of F1 occurs between 2005 and 2006, when it advances slightly. The mini-

mum extent of the total firn area (F1, F2 and F3) in the period summer 2003 to summer 2006 is reached in summer 2004. A large portion of SI is exposed along the transect. In 2003, several firn pockets (F2), between 1 and 3 m thick and with cross-sectional lengths of tens to hundreds of meter, likely originating from multiple years of firn accumulation, overly the SI (km 15-20). In 2004, no such pockets were identified, indicating that they have been melted away or transformed into SI. Figure 7 also indicates estimates of the ELA, inferred from mass balance stakes on Etonbreen, in the western part of the transect. The ELA decreased from 650 m in 2004, to 500 m in 2004 and 470 m in 2006. These elevations fall within the zone classified as SI in the corresponding year.

We also tracked characteristic IRHs within the firn over time. These represent previous year's summer surfaces. This analysis is not as robust as the mapping of glacier facies, but we found that the position of the IRHs in relation to the LSS remains apparently unchanged in the period spring 2004 to spring 2005. In subsequent years, the IRHs are progressively buried at a rate on the order of 1 m a^{-1}.

CONCLUDING REMARKS

Comparing the sequence of glacier-facies distribution with direct SMB measurements, we have to bear in mind some limitations on the information content of the mapped facies. Theoretically, the ELA corresponds to the lower boundary of the SI in a particular year. The fact that the ELAs from the mass balance stakes lie above the GPR-derived transition from SI to GI (Figure 7) illustrates the limitation of the GPR data to pin-point the exact position of the ELA. Even though SI can be identified from the GPR data, it remains undetermined whether this is old SI and subject to ablation, or newly formed SI that contributes positively to the SMB. A similar limitation applies for the detection of the recent firn line (the snow line by the end of the previous summer). In the case of a growing firn area, the firn line coincides with the lower boundary of the firn area. In case of a shrinking firn area, like in summer 2004, the recent firn line might retreat to a position within the multi-year firn (F1 and F2) and its determination may be ambiguous. Although the position of the ELA cannot directly be inferred from an individual facies distribution, its inter-annual variation is captured in the multi-year sequence.

The observed increase in the extent of the firn area, beginning in summer 2004, is in line with a lowering ELA, as derived from the mass balance stakes on Etonbreen over the same time period (Table 1). Between summer 2003 and summer 2006, the firn line lowered by about 40 to 100 m elevation in the north and west, and 150 to 230 m in the south and east of the ice cap, corresponding to a lateral expansion of the firn area along the profiles by up to 7.3 and 13.3 km, respectively. The apparently constant position of characteristic IRHs in spring 2004 and spring 2005 indicates that the entire winter snow has been heavily affected by summer melt, such that it is not recognizable in the GPR data. The concurrent disappearance of several firn pockets within the SI area provides further evidence of strong surface melt in summer 2004. This does not necessarily represent a complete absence of net accumulation, since it is likely that meltwater was retained through internal accumulation and SI formation.

This study demonstrates GPR as a non-destructive and useful tool to map glacier facies. Besides measuring the amount of winter snow, we obtained a multi-year sequence of glacier facies distribution. These can be interpreted in terms of SMB variations. In addition, these facies provide valuable ground-truth for validation and interpretation of satellite radar altimetry data, such as from Envisat or the upcoming CryoSat, another ESA satellite especially designed to monitor changes in the cryosphere.

ACKNOWLEDGEMENTS

This paper is a contribution to the International Polar Year project GLACIODYN, The Dynamic Response of Arctic glaciers to Global Warming and to the validation of CryoSat under direction of Duncan Wingham (UCL). The work was funded by the Norwegian Research Council, the Norwegian Space Center, the European Space Agency and the UK Natural Environment Research Council through grant NER/O/S/2003/00620. T. Dunse was supported through an Arktisstipend allocated by the Svalbard Science Forum. We thank Liz Morris (SPRI) for placing the neutron probe at our disposal and for assistance with the data, Geir Moholdt for his energetic dedication in the field (2006, 2007), Andrea Taurisano for collecting GPR data in 2004 and 2005 and Eirik Malnes (Norut) for geocoding the SAR scenes. Furthermore, we acknowledge numerous helpful comments by Kirsty Langley and the two reviewers, Anne Chapuis and Matthias Huss.

References

Bamber, J., W. Krabill, V. Raper and J. Dowdeswell, 2004. Anamolous recent growth of part of a large Arctic ice cap: Austfonna, Svalbard, *Geophysical Research Letters*, **31**, L12402.

Bevan, S., A. Luckman and T. Murray, 2007. Positive mass balance during the late 20th century on Austfonna, Svalbard revealed using satellite interferometry, *Annals of Glaciology*, **46**, 117–122.

Brandt, O., J. Kohler and M. Lüthje, 2008. Spatial mapping of multiyear superimposed ice on the glacier Kongsvegen, Svalbard, *Journal of Glaciology*, **54**(184), 73–80.

Dowdeswell, J.A., 1986. Drainage-basin characteristics of Nordaustlandet ice caps, Svalbard, *Journal of Glaciology*, **32**(110), 31–38.

Dowdeswell, J.A., B. Unwin, A.M. Nuttall and D.J. Wingham, 1999. Velocity structure, flow instability and mass flux on a large Arctic ice cap from satellite radar interferometry, *Earth and Planetary Science Letters*, **167**, 131–140.

Dunse, T., O. Eisen, V. Helm, W. Rack, D. Steinhage and V. Parry, 2008. Characteristics and small-scale variability of GPR signals and their relation to snow accumulation in Greenland's percolation zone, *Journal of Glaciology*, **54**(185), 333–342.

Hagen, J.O., T. Eiken, J. Kohler and K. Melvold, 2005. Geometry changes on Svalbard glaciers: mass-balance or dynamic response?, *Annals of Glaciology*, 255–261.

Hagen, J.O., O. Liestøl, E. Roland and T. Jørgensen, 1993. Glacier Atlas of Svalbard and Jan Mayen, Norsk Polarinstitutt, Oslo, Norway.

Hagen, J.O., K. Melvold, F. Pinglot and J.A. Dowdeswell, 2003. On the net mass balance of the glaciers and ice caps

in Svalbard, Norwegian Arctic, *Arctic Antarctic and Alpine Research*, 264–270.

Hagen, J.O. and N. Reeh, 2004. Mass Balance of the Cryosphere: Observations and Modelling of Contemporary and Future Changes, Bamber, J.L. and A.J. Payne, eds., In situ measurement techniques: land ice , Cambridge University Press, 11–41.

Hawley, R.L., O. Brandt, E.M. Morris, J. Kohler, A.P. Shepherd and D.J. Wingham, 2008. Instruments and Methods. Techniques for measuring high-resolution firn density profiles: a case study from Kongsvegen, Svalbard, *Journal of Glaciology*, **54**, 463–468.

IPCC, 2007. Climate Change 2007: The Physical Sience Basis. Summary for Policymakers. Contribution of Working Group I to the Fourth Assessment Report of the Intergovernmental Panel on Climate Change.

Kohler, J., J. Moore, M. Kennett, R. Engeset and H. Elvehøy, 1997. Using ground-penetrating radar to image previous years' summer surfaces for mass-balance measurements, *Annals of Glaciology*, **24**, 355–360.

König, M., J. Wadham, J.G. Winther, J. Kohler and A.M. Nuttall, 2002. Detection of superimposed ice on the glaciers Kongsvegen and midre Lovenbreen, Svalbard, using SAR satellite imagery, *Annals of Glaciology*, **34**, 335–342.

Kovacs, A., A.J. Gow and R.M. Morey, 1995. The in-situ dielectric constant of polar firn revisited, *Cold Regions Science and Technology*, **23**, 245–256.

Langley, K., 2007. Glacier Subsurface Interpretation Combining Ground Penetrating Radar and Satellite Synthetic Aperture Radar, Ph.D Thesis, vol. 645, Faculty of Mathematics and Natural Sciences, University of Oslo.

Langley, K., S.E. Hamran, Høgda, K.A., R. Storvold, O. Brandt, J.O. Hagen and J. Kohler, 2007. Use of C-band ground penetrating radar to determine backscatter sources within glaciers, *IEEE Transactions on Geoscience and Remote Sensing*, **45**, 1236–1246.

Lauknes, I. and E. Malnes, 2004. Automatical geocoding of SAR products, Lacoste, H. and L. Ouwehand, eds., Envisat and ERS Symp., Salzburg, Austria, Sep. 6-10, 2004, CD–ROM.

Morris, E.M., 2008. A theoretical analysis of the neutron-scattering method for measuring snow and ice density, *Journal of Geophysical Research*, **113**, F03019.

Morris, E.M. and J.D. Cooper, 2003. Density measurements in ice boreholes using neutron scattering, *Journal of Glaciology*, **49**(167), 599–604.

Paterson, W.S.B., 1994. The Physics of Glaciers, Elsevier Science Ltd, Oxford, UK, third ed.

Pinglot, J.F., J.O. Hagen, K. Melvold, T. Eiken and C. Vincent, 2001. A mean net accumulation pattern derived from radioactive layers and radar soundings on Austfonna, Nordaustlandet, Svalbard, *Journal of Glaciology*, **47**(159), 555–566.

Schuler, T.V., E. Loe, A. Taurisano, T. Eiken, J.O. Hagen and J. Kohler, 2007. Calibrating a surface mass balance model for the Austfonna ice cap, Svalbard, *Annals of Glaciology*, **46**, 241–248.

Scott, J.B.T., P. Nienow, D. Mair, , V. Parry, E. Morris and D.J. Wingham, 2006. Importance of seasonal and annual layers in controlling backscatter to radar altimeters across the percolation zone of an ice sheet, *Geophysical Research Letters*, **33**, L24502.

Shepherd, A. and D. Wingham, 2007. Recent Sea-Level Contributions of the Antarctic and Greenland Ice Sheets, *Science*, **315**(5818), 1529–1532.

Taurisano, A., T.V. Schuler, J.O. Hagen, T. Eiken, E. Loe, K. Melvold and J. Kohler, 2007. The distribution of snow accumulation across the Austfonna ice cap, Svalbard: direct measurements and modelling, *Polar Research*, **26**, 7–13.

Wadham, J., J. Kohler, A. Hubbard, A.M. Nuttall and D. Rippin, 2006. Superimposed ice regime of a high Arctic glacier inferred using ground-penetrating radar, flow modeling, and ice cores, *Journal of Geophysical Research*, **111**, F01007.

Wingham, D.J., R. Forsberg, S. Laxon, P. Lemke, H. Miller, K. Raney, S. Sandven, R. Scharroo, P. Vincent and H. Rebhan, 2001. CryoSat calibration and validation concept, *Tech. rep.*, ESA.

Woodward, J., M. Sharp and A. Arendt, 1997. The influence of superimposed-ice formation on the sensitivity of glacier mass balance to climate change, *Annals of Glaciology*, **24**, 186–190.

Zwally, H.J., M.B. Giovinetti, J. Li, H.G. Cornejo, M.A. Beckley, A.C. Brenner, J.L. Saba and D. Yi, 2005. Mass changes of the Greenland and Antacrctic ice sheets and shelves and contributions to sea-level rise: 1992-2002, *Journal of Glaciology*, **51**(175), 509–527.

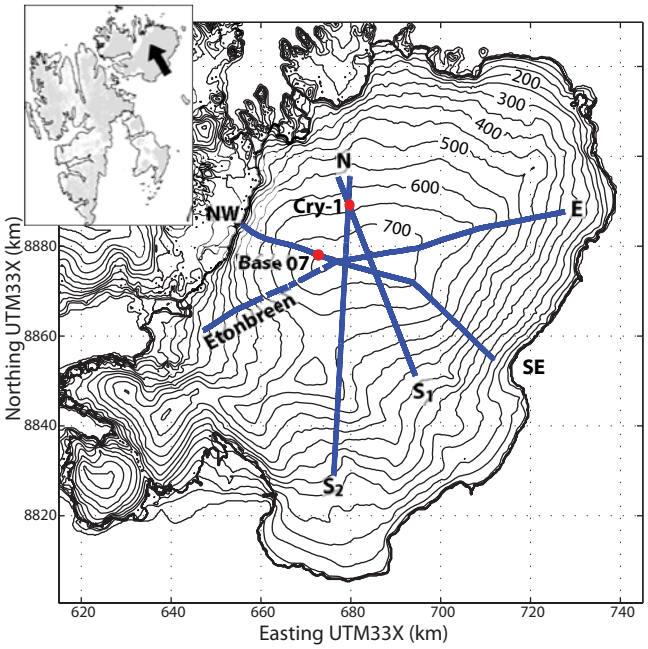

Fig. 1. Map of the Austfonna ice cap on Nordaustlandet. The blue lines indicate the GPR transects measured in 2007, while the red markers show the location of the basecamp in 2007 and of study site Cry-1. The insert shows the location of Nordaustlandet within the Svalbard archipelago.

Table 1. Approximate firn-line elevations along the GPR profiles from end-of-summer 2003 to 2006, total change during that period and corresponding lateral expansion. In addition, estimates of the ELA from mass balance stakes on Etonbreen are given.

Profile *	Firn-line elevation (m) †				Difference (m)	Expansion (km)
	2003	2004	2005	2006	2006−2003	2003 to 2006
Eton ELA	–	650	500	470	180	8.5
Eton	650	660	590	550	100	5.2
NW	680	720	650	640	40	1.9
N ‡	650	650	550	–	100	7.3
E	620	640	500	390	230	13.1
SE	600	–	540	450	150	6.1
S_1	650	–	490	440	210	13.3
S_2	650	–	–	500	150	10.6

*see figure 1 for profile locations
†no differentiation has been made, whether or not the firn originates from the previous year
‡Diff. and Exp. referrer to period 2003 to 2005, firn line in 2006 beyond end of GPR transect

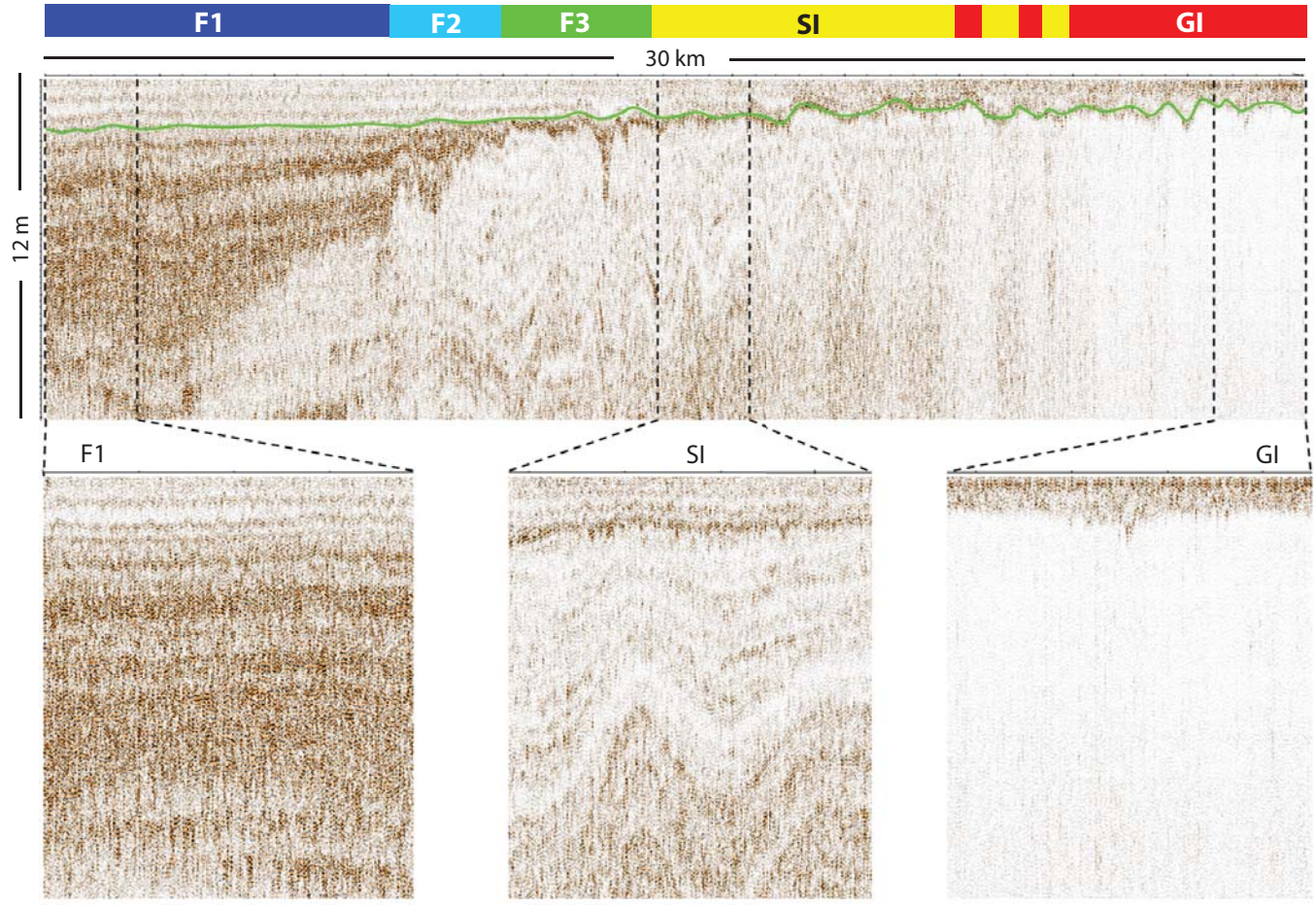

Fig. 2. GPR classification of glacier facies along a 30 km long transect from the summit area (F1) into the ablation area (GI) of Etonbreen. The green line indicates the position of the LSS. The Lower panels show close ups of 2 km GPR data with characteristic signal-reflection patterns.

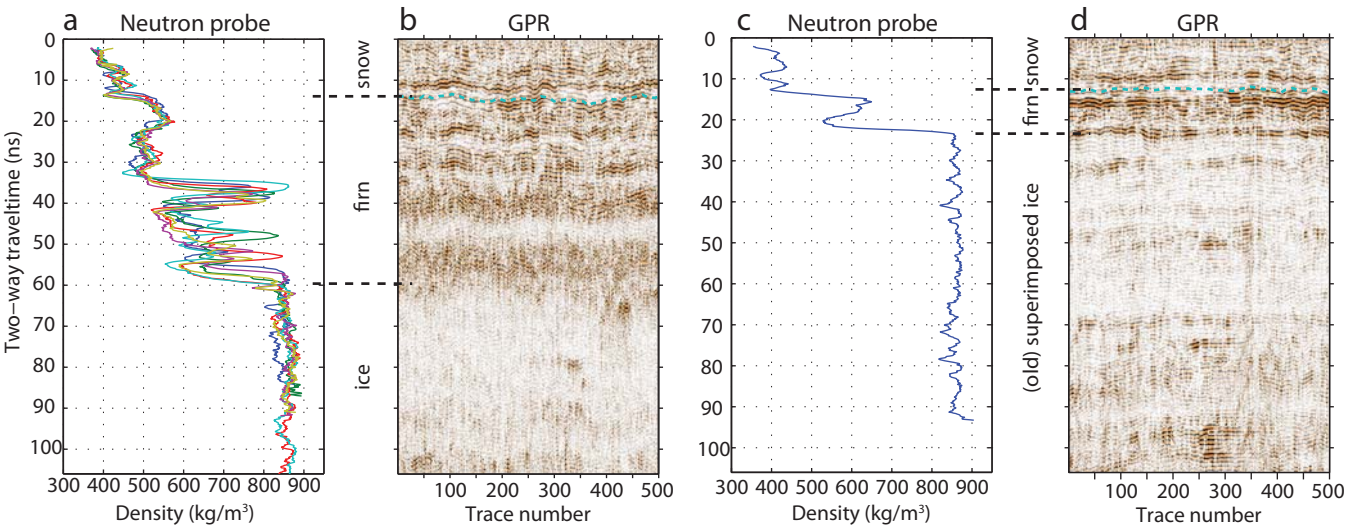

Fig. 3. Comparison of vertical density profiles, inferred from neutron-scattering probing with GPR signal reflections obtained along ∼120 m sections at Base 07 (a,b) and Cry-1 (c,d). The dashed lines in the GPR images indicate the position of the LSS as confirmed from snow pits and manual snow-depth soundings.

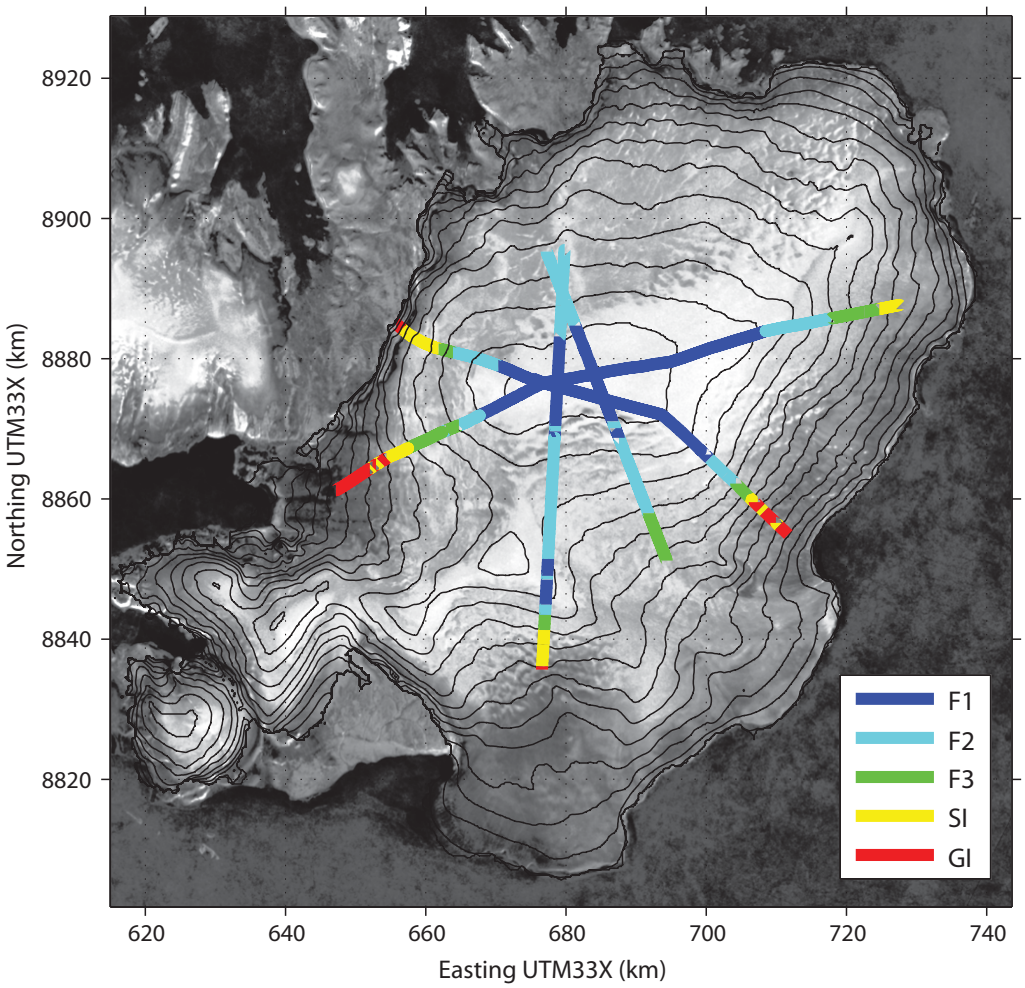

Fig. 4. Comparison of GPR-derived glacier facies distribution in summer 2006 with a 2-D backscatter SAR image. The image is an average of a number of winter scenes acquired in 2005 to 2007.

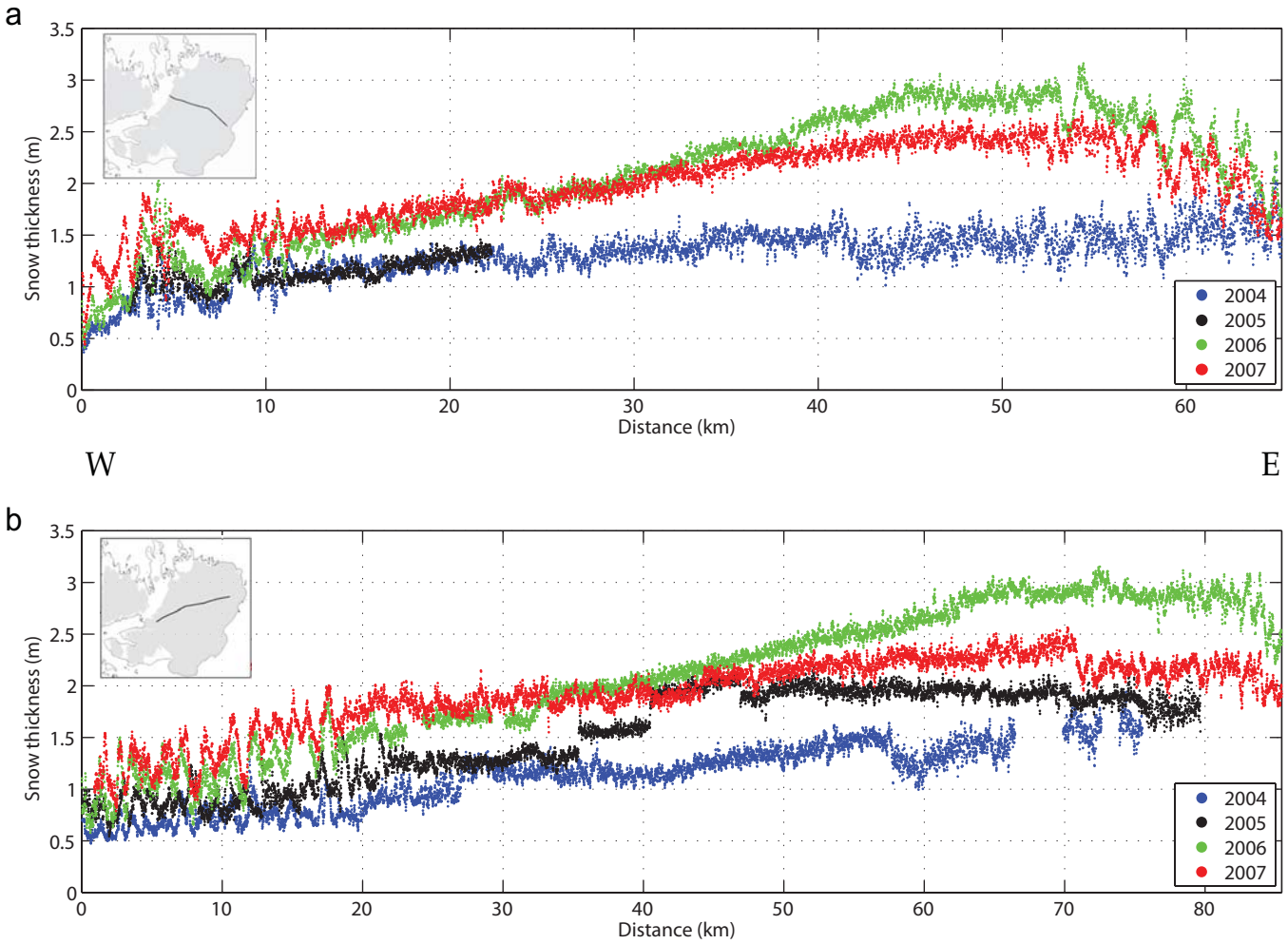

Fig. 5. Snow thickness profiles for spring 2004 to 2007, a) along the NW-SE and b) SW-E transect.

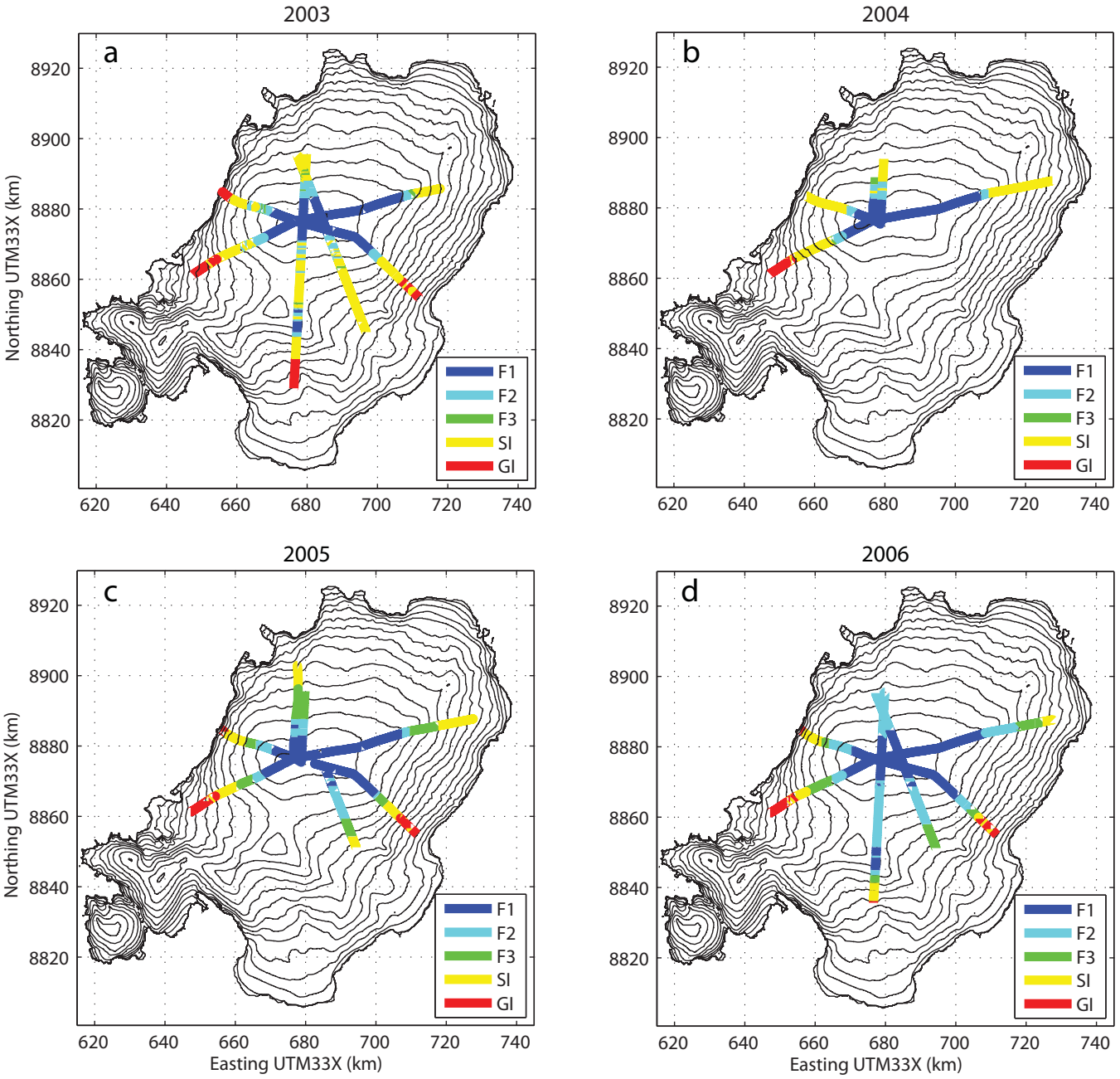

Fig. 6. Colour-coded glacier facies in end-of-summer 2003 to 2006 along the GPR transects in spring 2004 to 2007, plotted on top of a contour map of Austfonna with 50 m contour interval.

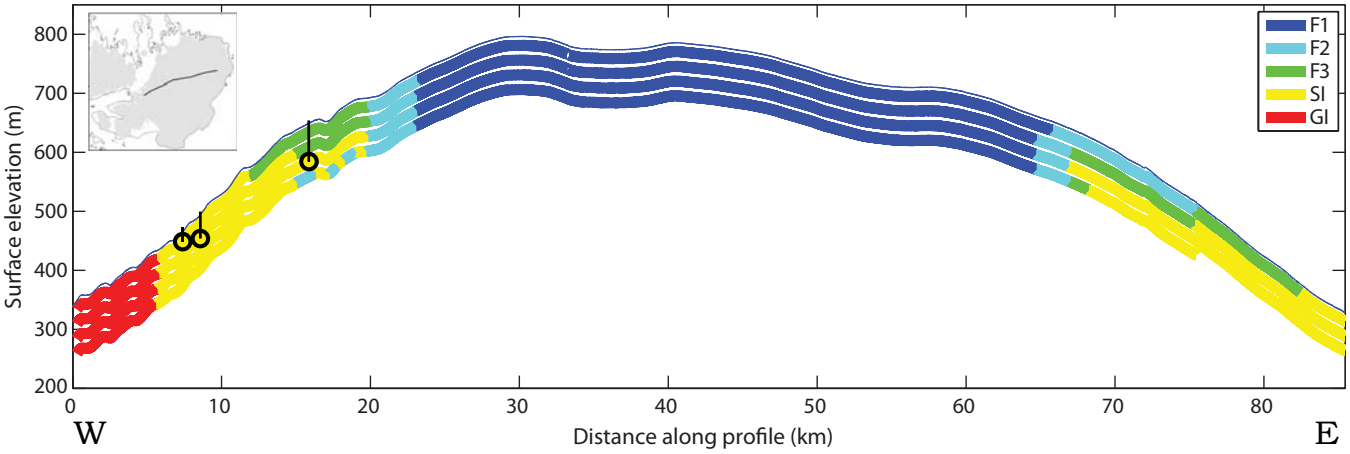

Fig. 7. Colour-coded glacier facies along the transect from Etonbreen in the west via the summit area towards the east. Each stripe represents the classification for a particular year in chronological order with 2006 at the top and 2003 at the base. Note that the thickness of the stripes are not related to the actual snow thickness or depth. Black markers indicate ELA estimates inferred from mass balance stakes on Etonbreeen for 2004 to 2006.